Available online at www.sciencedirect.com

ScienceDirect

Procedia CIRP 111 (2022) 302–307

www.elsevier.com/locate/procedia

12th CIRP Conference on Photonic Technologies [LANE 2022], 4–8 September 2022, Fürth, Germany

# Direction-independent temperature monitoring for Laser Metal Deposition with coaxial wire feeding

Avelino Zapata[a,*], Christian Bernauer[a], Melanie Hell[a], Helmut Kriz[b], Michael F. Zaeh[a]

[a]*Technical University of Munich, Institute for Machine Tools and Industrial Management, Boltzmannstr. 15, 85748 Garching, Germany*
[b]*Sensortherm GmbH, Weißkirchener Straße 2-6, 61449 Steinbach, Germany*
* Corresponding author. Tel.: +49 89 289 15572; fax: +49 89 289 15444. *E-mail address:* avelino.zapata@iwb.tum.de

**Abstract**

Among the Directed Energy Deposition (DED) processes, Laser Metal Deposition with wire (LMD-w) combines the advantages of a high precision and a high deposition rate. Recently, optical systems have been developed that allow to coaxially feed the wire through the center of a hollow laser beam into the induced melt pool. When a pyrometer is coupled to such an optical system, the measurement spot features the same annular shape as the laser spot. In this work, the temperature signal of such a setup was studied and the system was qualified for inline process monitoring. The size of the measurement spot was systematically varied, and the temperatures that resulted from the two modalities of a one-color as well as a two-color measurement were compared. It was shown that the size of the annular measurement spot significantly influences the temperature signal for both modalities. A better understanding of the measurement is essential to monitor the process reliably.



*Keywords:* pyrometry; Directed Energy Deposition; Laser Metal Depositon; annular laser beam; process monitoring

## 1. Introduction

Directed Energy Deposition (DED) processes become increasingly important for Additive Manufacturing (AM) since they facilitate the production of large freeform parts at high material deposition rates [1]. The laser-based DED processes, also called Laser Metal Deposition (LMD) processes, allow a focused and precise energy input and are therefore a promising AM technology for the manufacturing of near-net-shape parts [2]. When a wire is used as feedstock in LMD, it is often fed laterally to the process, resulting in a leading or trailing configuration, depending on the movement direction. A coaxial alignment of the laser beam and the wire, which allows a direction-independent process, can be achieved with specialized optics that form a laser beam with an annular profile [3]. The process temperature is crucial for all DED processes because it affects the geometrical and mechanical properties of the produced parts. It is, therefore, of particular interest for in-situ process monitoring and control [4].

Contactless temperature measurement methods such as pyrometry can be flexibly integrated into production systems and are oftenä used to measure the melt pool temperatures. By coupling the pyrometer directly to the optical system, the same path of the laser beam can be used. The resulting annular measuring spot allows an in-axis measurement. However, the temperature signals that result from this setup have not yet been studied. To monitor the process reliably, a better understanding of the measurement is essential.

## 2. Fundamentals and state of the art

### *2.1. Fundamentals*

Planck's law precisely describes the radiance of a surface depending on the temperature and the wavelength. However, Wien's approximation to Plank's law is more commonly used to formulate this dependency for technical purposes because of its simplicity. The spectral radiance for a black body $I_{b,\lambda}$

2212-8271 
10.1016/j.procir.2022.08.027

calculated with Wien's approximation differs from the one calculated with Planck's law by less than 1 % if $\lambda \cdot T <$ 3125 µm K, which can be assumed to be fulfilled for the investigations described in the following, with $\lambda$ being the wavelength and $T$ being the temperature [5]. For a black body, Wien's approximation can be written as

$$I_{\mathrm{b},\lambda}(\lambda, T) = \frac{c_1}{\lambda^5} \cdot \frac{1}{e^{\frac{c_2}{\lambda \cdot T}}} \quad (1)$$

with the radiation constants $c_1 = 1.191 \times 10^{-16}$ W m$^2$ sr$^{-1}$ and $c_2 = 1.439 \times 10^{-2}$ m K [6]. Since a black body represents an ideal object, the ratio between the radiance from a real body and a black body, described by the spectral directional emissivity $\varepsilon_\lambda$, is needed to calculate the temperature based on the radiance of a real body [7]:

$$\varepsilon_\lambda(\lambda, T, \theta, \phi) = \frac{I_\lambda(\lambda, T, \theta, \phi)}{I_{\mathrm{b},\lambda}(\lambda, T)} \quad (2)$$

The zenith angle $\theta$ and the azimuth angle $\phi$ are introduced to consider direction-dependent surface radiation properties. However, it would be impractical to presuppose the knowledge of the exact spectral directional emissivity for calibration purposes. Therefore, assumptions are introduced. First, it can be assumed that the radiance is measured at a sufficiently narrow wavelength range, so the dependence of $\lambda$ is neglectable. Next, the viewing direction is usually static during the measurement. Hence, the dependency of the angles $\theta$ and $\phi$ is not considered. Moreover, if the temperature range of interest is small, a constant emissivity can be assumed. Therefore, most commercially available contactless temperature measurement systems are calibrated by tuning the simplified constant emissivity $\varepsilon$.

### *2.2. State of the art*

The use of a known reference temperature at the measurement spot is one of the established methods for calibrating the emissivity. Thermocouples can be utilized for this purpose [8]. Another option is the evaluation of measured cooling curves to identify temperature plateaus that result from known phase transitions to infer the temperature [9]. The visible transition from liquid to solid can also be used in this context [10]. Other methods involve evaluating spectroscopical data or the calculation based on sophisticated emissivity models [11,12]. For two-color measurements, emissivity is considered differently. Since the radiance is measured at two channels with the different wavelengths $\lambda_1$ and $\lambda_2$, the temperature is calculated using an emissivity ratio $\varepsilon_r = \varepsilon_1/\varepsilon_2$ [5]. Under certain conditions, the emissivity ratio offers advantages for the temperature measurement. First, if the condition $\varepsilon_1 \approx \varepsilon_2$ is satisfied, the calculated temperature is independent of the emissivity of the body. Second, if $\varepsilon_1/\varepsilon_2$ is constant for the temperature range of interest, the temperature measurement is not influenced by process disturbances that affect the radiance at both wavelengths [13]. Third, the temperature of objects smaller than the pyrometer spot can be measured because the temperature obtained with this method approximately corresponds to the highest temperature within the measurement area [14]. The same advantages result in multi-color measurements [15].

In the studies mentioned, suitable emission coefficients were determined for the respective setups and materials. However, a direct transferability of the identified emissivities to new applications is only restrictively possible since numerous factors alter the emissivity for a given setup [16]. Pyrometers are frequently used in LMD to measure the temperature in the melt pool [17]. It was shown that the geometry of the part and the degree of surface oxidation influence the measurement [18]. Another study demonstrated that the position of the measurement point within the melt pool significantly affects the measured temperature [19]. An additional study took this advantage to simultaneously measure the temperatures at the center and the rear part of the melt pool to determine a cooling rate [20].

## 3. Objective and approach

In the coaxial LMD process with wire, the wire is fed to the center of the melt pool. Hence, for the widely implemented lateral alignment of the pyrometer, the measurement spot of the pyrometer, the *pyrometer spot*, needs to be positioned on an area next to the wire. This area is located in the front, the side, or the rear part of the melt pool, depending on the movement direction of the process. Different temperatures are present in the distinct areas of the melt pool. Therefore, a direction-independent temperature measurement is challenging. A solution is the direct coupling of the pyrometer into the optical system so that the resulting pyrometer spot has the same annular shape as the laser spot. This special shape allows identical measurement conditions for any lateral movement direction. However, it is not well understood how the annular shape and the increased size of the pyrometer spot as well as the wire impact the temperature signal. Therefore, the temperature signals resulting from different measurement setups were analyzed in this work. At first, a practical method for the pyrometer calibration was implemented. Then, three different sizes of the measurement spot were investigated for the temperature measurement of processes with and without wire feed. Based on the resulting temperature signals, the influence of the pyrometer spot size and the wire was examined. Finally, the temperature signal for a multi-directional process was evaluated.

## 4. Experimental

### 4.1. Systems

The coaxial deposition head (CoaxPrinter, Precitec GmbH & Co. KG, Germany) reshaped the laser beam through a combination of axicons to obtain a hollow laser beam resulting in an annular beam profile. The laser beam source was an 8-kW multi-mode fiber laser (YLR-8000, IPG Laser GmbH, Germany) emitting at a wavelength of 1070 nm. The feedstock was provided by an industrial wire feeding unit (DIX FDE-PN 100 L, DINSE GmbH, Germany). For the temperature measurement, a two-color (quotient) pyrometer (METIS M322, Sensortherm GmbH, Germany) with a temperature measurement range between 600 and 2300 °C and a response

time of 1 ms was coupled to the optical system (see Fig. 1a). The spectral ranges of the first and the second channel (C1 and C2) were 1.65–1.80 µm and 1.45–1.65 µm, respectively. This pyrometer allowed simultaneous one-color and two-color measurements. The heat source (HE1200, Sensortherm GmbH, Germany) with an adjustable temperature between 100 and 1100 °C together with an attachable iris diaphragm were used for the calibration (see Fig. 1b).

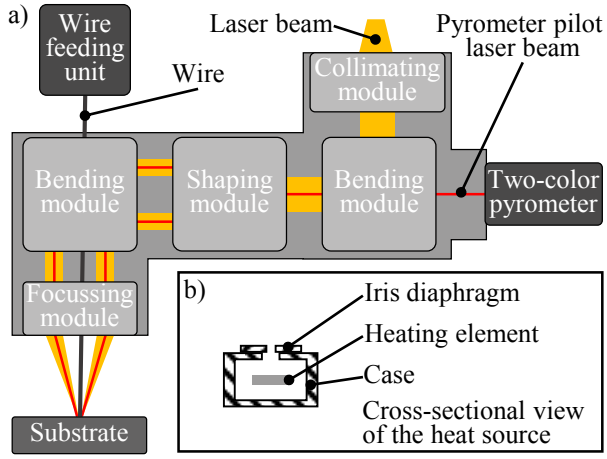


Fig. 1. a) Schematic illustration of the experimental setup and b) cross-sectional view of the heat source.

### 4.2. Materials

AISI 304 substrate plates (100 mm × 100 mm) with a thickness of 10 mm and an AISI 308L wire with a diameter of 1 mm were used in the experiments. The chemical composition of both materials is shown in Table 1.

Table 1. Chemical composition of the substrate plates (AISI 304) and the wire (AISI 308L) by mass percentage

| Alloy | Alloying elements by mass percentage |
|---|---|
| AISI 304 | C ≤ 0.07; Si ≤ 1.00; Mn ≤ 2.00; P ≤ 0.05<br>S ≤ 0.02; Cr 17.50–19.50; Ni 8.00–10.50 |
| AISI 308L | C ≤ 0.03; Si 0.65–1.20; Mn 1.00–2.50; P ≤ 0.03<br>S ≤ 0.02; Cr 19.00–21.00; Ni 9.00–11.00 |

### 4.3. Methods

The method used for calibration is based on melting the surface of the material with the least possible energy input so that the melting temperature is just reached or only marginally exceeded. A homogeneous temperature distribution can be assumed in a small melt pool and steadier surface conditions (e.g., less fluctuation of the liquid surface, which would lead to a dynamic radiation character) can be expected. Therefore, the laser beam and the pyrometer spot were concentrically aligned and focused on the surface of the substrate plate, resulting in a solid circular laser and pyrometer spot. Single tracks with a length of 80 mm were produced, where only the laser beam source was engaged, and no additional material was fed to the surface. The laser power $P_L$ was increased by 50 W for every track, from 50 W to 250 W, and the traverse speed was set to 3 m min$^{-1}$. The surface of the substrate plate was then analyzed with a profilometer to examine at which laser power the first signs of melting could be identified. It was assumed that the temperature within the pyrometer spot was approximately equal to the melting temperature for the tracks where the first continuous melting occurred. The emissivities used for the one-color measurements and the emissivity ratio used for the two-color measurement were then adjusted so that the indicated temperature was equal to the melting temperature. A melting temperature of 1450 °C was chosen based on the melting ranges of both the substrate plate and the wire material.

For further experiments, the working distance of the optical system was changed to achieve an annular laser spot on the surface of the substrate plate that allowed the coaxial wire feed. The distance between the surface of the substrate plate and the focal plane of the laser, the *focal offset*, determines the size of the annular laser spot. A −6 mm focal offset (with the focal plane below the surface of the substrate plate) was chosen, resulting in an annular laser spot with an inner diameter $d_i$ of 1.2 mm and an outer diameter $d_o$ of 2.6 mm. By means of individual focusing units, it was possible to adjust the size of the pyrometer spot without altering the size of the laser spot. An iris diaphragm was used to determine the dimensions of the pyrometer spot. For this purpose, the pyrometer was pointed onto the heating element within the heat source and the iris diaphragm was placed in between with a fully opened aperture. By gradually closing the aperture, the diaphragm progressively intersected the radiance detected by the pyrometer. The reduction of the measured radiance lowered the perceived temperature and, thus, allowed to determine the boundaries of the3yrometerr spot. Because the temperature change occurred gradually, a threshold of 95 % of the initial temperature was chosen to define the boundaries. Three pyrometer spot sizes (small, medium-sized, and large) were set for the temperature measurement. The sizes of the corresponding inner diameters and the outer diameters are illustrated in Fig. 2.

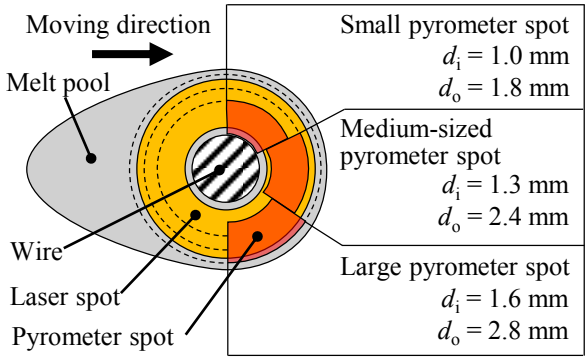


Fig. 2. Schematic illustration of the measurement setup for a small, a medium-sized, and a large annular pyrometer spot.

The temperatures $T_{C1}$ and $T_{C2}$ resulting from the one-color measurements and the temperature $T_Q$ resulting from the two-color measurement were observed in the experiments. Based on previous studies, a laser power of 1600 W and a traverse speed of 1 m min$^{-1}$ were chosen for the experiments [21].To analyze the influence of the additional wire feed on the temperature measurement, the experiments were first conducted without wire feed and then with a wire speed of 1 m min$^{-1}$. Lastly, the same parameter settings were used to build a thin-walled square geometry consisting of ten layers and a side length of 35 mm while measuring the temperature.

## 5. Results and discussion

### 5.1. Emissivity calibration

The three height profiles of the surfaces of the tracks produced with laser powers of 100 W, 150 W, and 200 W are depicted in Fig. 3. For a laser power of 100 W, only a small change of the surface topography at the laser spot path is visible. The small change indicates that the melting temperature of the material was not continuously reached. A continuous line with a smoother surface than the surface of the substrate plate was visible in the height profile of the track produced with a laser power of 150 W. Here it was assumed that a temperature close to the melting temperature was consistently reached on the surface. A laser power of 200 W led to a broader track. Hence, it was assumed that the temperature during this process was higher than the melting temperature. Therefore, a laser power of 150 W was selected to determine the emissivity.

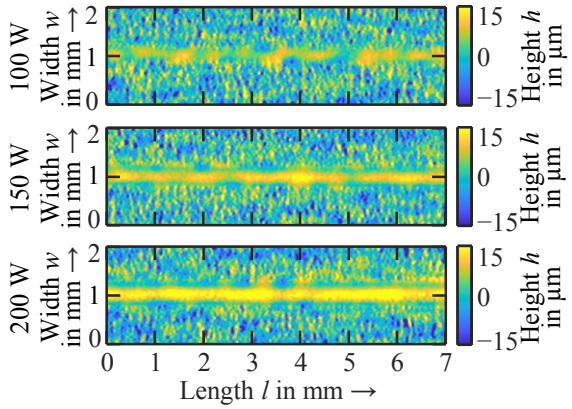


Fig. 3. Height profiles of the substrate plates for laser powers of 100 W, 150 W, and 200 W.

Multiple tracks were produced with the identified parameter combination while measuring the temperature. The laser started to emit 0.8 s before the traverse movement was activated. This initial static phase facilitated stable starting conditions during the experiments with wire feed. By changing the value of the emissivity in the software of the pyrometer, the calculated temperature was adjusted. The measured temperatures with the independently identified $\varepsilon_1 = 0.75$, $\varepsilon_2 = 0.85$, and $\varepsilon_r = 1.18$ are shown in Fig. 4. The diagram shows that $T_{C1}$ and $T_{C2}$ rose over 1600 °C as soon as the laser was activated. The temperature increased during the static phase to approximately 2200 °C and rapidly decreased as soon as the laser spot was moved. During the movement phase, the mean $T_{C1}$ and $T_{C2}$ were 1450 °C, with a $T_{C2}$ on average 7 K higher than $T_{C1}$. $T_Q$ deviated from $T_{C1}$ and $T_{C2}$ substantially and was below the melting temperature during the static and the beginning of the movement phase. This unexpected temperature deviation resulted from the different emissivities during the static and the movement phase caused by the different mean temperatures and surface conditions of the melt pool. The changes of $\varepsilon_1$ and $\varepsilon_2$ are indicated by the inconstant difference between $T_{C1}$ and $T_{C2}$. Because $T_Q$ strongly depends on a constant emissivity ratio, the highest differences between $T_Q$ and $T_{C1}$ as well as between $T_Q$ and $T_{C2}$ occurred during periods with a relatively high or low agreement between $T_{C1}$ and $T_{C2}$. Only during the movement phase, where the difference between $T_{C1}$ and $T_{C2}$ was approximately constant, $T_Q$ yielded plausible temperature values. During most of the movement phase, all three temperatures approximately matched.

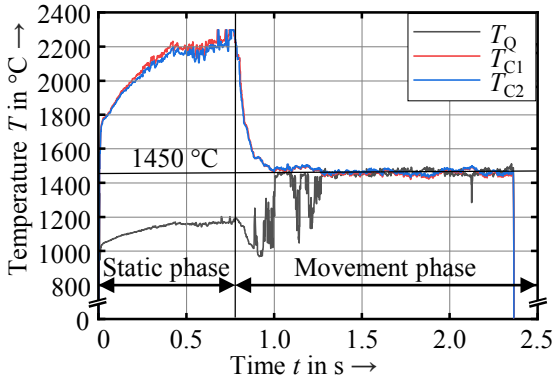


Fig. 4. Temperature curves for the track with a laser power of 150 W and $\varepsilon_1 = 0.75$, $\varepsilon_2 = 0.85$, and $\varepsilon_r = 1.18$.

### 5.2. Temperature signals

All temperature diagrams in Fig. 5 show that during the static phase $T_{C1}$ and $T_{C2}$ rose from 1600 to 1800 °C, while $T_Q$ dropped from over 2000 to 1000 °C. This temperature drop can be explained analogously to the findings in section 5.1. The static phase was excluded in the analysis of the temperature signals to focus on the movement phase. The comparative results of the measured temperatures for the chosen process parameters (see section 4.3) are summarized in Table 2.

Table 2. Summary of the temperature measurement; fluctuations (alternated, repeated positive and negative value changes within fractions of a second) in the temperature of less than 50 K are categorized as *low*, fluctuations between 50 K and 300 K as *medium*, and fluctuations above 300 K as *high*.

| Pyrometer spot size | Use of wire | Mean $T_{C1}$ in °C | Mean $T_{C1}$–$T_{C2}$ in K | Mean $T_Q$ in °C | Fluctuation of $T_{C1}$ and $T_{C2}$ | Fluctuation of $T_Q$ |
|---|---|---|---|---|---|---|
| Small | No | 1630 | 7 | 1520 | Low | High |
| Small | Yes | 1620 | 7 | 1550 | Medium | High |
| Medium | No | 1600 | 15 | 1728 | Low | Medium |
| Medium | Yes | 1570 | 15 | 1710 | Low | Medium |
| Large | No | 1490 | 40 | 2060 | Low | Medium |
| Large | Yes | 1450 | 40 | 2110 | Low | Medium |

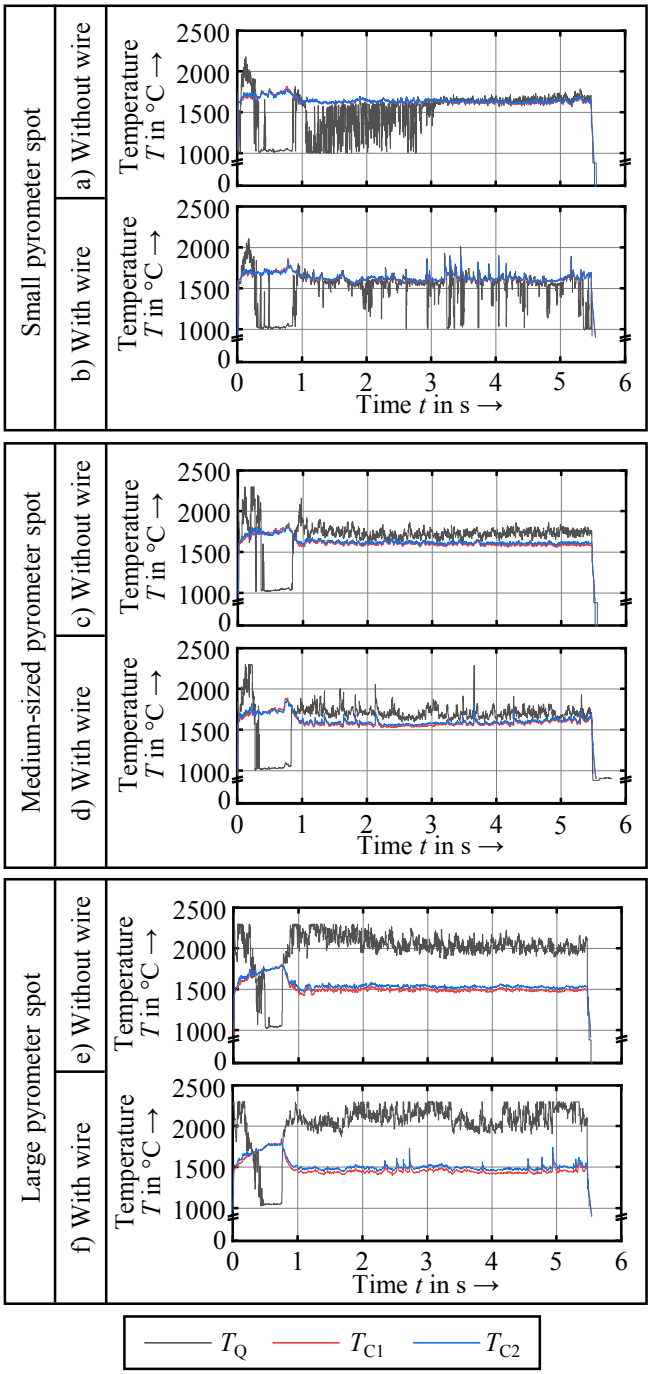


Fig. 5. Temperature curves for a small (a and b), a medium-sized (c and d), and a large pyrometer spot (e and f)

*Small pyrometer spot:* The best agreement of $T_{C1}$, $T_{C2}$, and $T_Q$ was achieved with the smallest pyrometer spot. An increased difference between $T_{C1}$ and $T_{C2}$ is an indicator for wavelength-dependent changes in the emissivity with regard to the calibrated emissivities. Since the small pyrometer spot covered the smallest measurement area, only minor wavelength-dependent emissivity differences due to temperature gradients or surface conditions arose.

*Medium-sized pyrometer spot:* Because the medium-sized pyrometer spot covered greater areas of the melt pool, larger wavelength-dependent emissivity differences resulted. The different emissivities led to a slightly higher difference between $T_{C1}$ and $T_{C2}$ of 8 K than the small pyrometer spot. $T_Q$ was also affected by the resulting change in the emissivity ratio, showing higher mean temperatures than the one-color measurements.

*Large pyrometer spot:* The highest difference between $T_{C1}$ and $T_{C2}$ as well as a high increase in $T_Q$ resulted for the temperature measurements with the large pyrometer spot. The comparably high value of $T_Q$ is unlikely to result from the melt pool temperature since the large pyrometer spot covered the areas closer to the edge of the melt pool, where lower temperatures could be expected. $T_{C1}$ and $T_{C2}$ show the expected slightly lower temperatures than the measurements conducted with the other pyrometer spot sizes. Overall, the one-color measurements were less sensitive to the changing conditions and showed fewer temperature fluctuations.

*Influence of the wire:* When comparing the diagrams that resulted from measurements conducted with the same pyrometer spot size, but for a process with and without wire, irregularities in the form of sudden temperature peaks are visible in the process with wire. These temperature peaks are unlikely to result from the melt pool temperature. Therefore, it can be assumed that small vibrations of the wire caused a temporal intersection with the pyrometer spot, which abruptly changed the radiance conditions and thus the perceived temperature. This effect was mainly observed in the measurements with the small pyrometer spot, where the inner diameter of the pyrometer spot was equal to the diameter of the wire. The temperature fluctuations in the measurements with the medium-sized and large pyrometer spots show fewer peaks. The larger distance between the pyrometer spot and the wire prevented that small displacements of the wire caused an intersection. It can be assumed that most of the vibration of the wire occurred within a circle with a diameter of 1.3 mm, corresponding to the inner diameter of the medium-sized pyrometer spot.

### 5.3. Multi-directional process

The temperature during the multi-directional build-up process was studied using a one-color measurement (C1) and the medium-sized pyrometer spot. A progressive increase from an average $T_{C1}$ of 1700 °C at the start to 1800 °C at the end was measured (Fig. 6a). The temperature signal shows periodic temperature changes that were attributed to the trajectory of the process. Analyzing the temperature during the second layer indicated that the temperature systematically rose when the process approached the corners (Fig. 6b and 6c). The temperature increase can be explained by heat accumulation effects resulting from the direction change in the corners. After the corners, the temperature decreased and repeatedly reached local minima in the center section of each side. The temperature in these center sections increased for each section indicating the5rogresssive heating of the substrate plate as well as the melt pool temperature. Through the similarity of the temperature progressions at each side it was demonstrated that the different movement directions had no affect on the measurement.

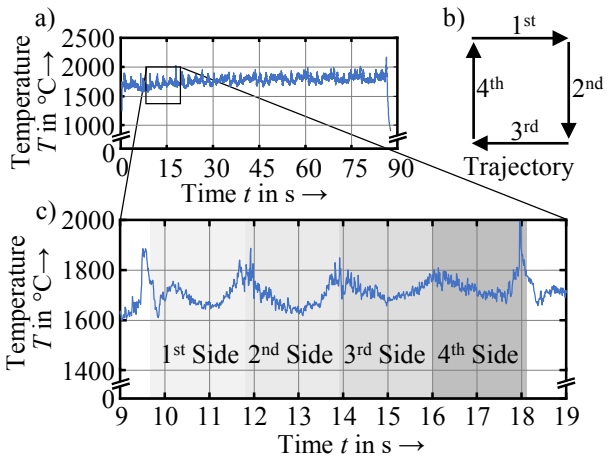


Fig. 6. A) Temperature signal during the multi-directional build-up process of ten consecutive layers, b) trajectory of the multi-directional process, c) detailed view of the signal during the buid-up of the second layer.

## 6. Conclusion

This work investigated the influence of different pyrometer setups for the coaxial temperature measurement of a Laser Metal Deposition process with wire. After adapting and implementing a practical method for the calibration of the pyrometer and conducting experiments while varying the size of an annular pyrometer spot, the following conclusions could be drawn:

- Identifying the emissivity of a melt pool based on the process temperature at the transition from a solid to a liquid phase led to plausible temperature values for one-color measurements.
- The wavelength-dependent changes of the emissivity of different areas of the melt pool led to significant uncertainties in the case of two-color measurements.
- Process-induced wire vibrations resulted in rapid changes in the temperature signal when the wire intersected with the pyrometer spot.
- The melt pool temperature can be measured for alternating movement directions utilizing an annular pyrometer spot.

The evaluation of the melt pool temperature is crucial to detect an overheating that would negatively affect the geometrical and mechanical properties of the produced part. Therefore, in future studies, the setup will be used to monitor the temperature during a multi-layer additive process. Also, the application for temperature control will be addressed.

## Acknowledgments

This study was carried out using systems provided by the Precitec GmbH & Co. KG, Sensortherm GmbH, and DINSE GmbH. We thank our partners for entrusting us with the systems and the excellent cooperation. We also thank the German Federal Ministry of Education and Research (BMBF) for funding this reasearch within the KORESIL project with the grant number 02P20Z002 and we thank the Projektträger Karlsruhe (PTKA) for the supervision.

## 7. References

[1] DebRoy T, Wei HL, Zuback JS, Mukherjee T, Elmer JW, Milewski JO, Beese AM, Wilson-Heid A, De A, Zhang W. Additive manufacturing of metallic components – Process, structure and properties. Prog. Mater. Sci. 2018; 92: pp. 112–224.
[2] Dass A, Moridi A. State of the Art in Directed Energy Deposition: From Additive Manufacturing to Materials Design. Coatings 2019; 9: #418.
[3] Kelbassa J, Biber A, Wissenbach K, Gasser A, Pütsch O, Loosten P, Schleifenbaum JH. Influence of focal length on the laser metal deposition process with coaxial wire feeding. Proc. SPIE 2019; 10911: pp. 1–12.
[4] Everton SK, Hirsch M, Stravroulakis P, Leach RK, Clare AT. Review of in-situ process monitoring and in-situ metrology for metal additive manufacturing. Mater. Des. 2016; 95: pp. 431–445.
[5] Müller B, Renz U. Development of a fast fiber-optic two-color pyrometer for the temperature measurement of surfaces with varying emissivities. Rev. Sci. Instrum. 2001; 72: pp. 3366–3374.
[6] Mohr PJ, Taylor BN, Newell DB. CODATA recommended values of the fundamental physical constants: 2010. Rev. Mod. Phys. 2012; 84: pp. 1527–1605.
[7] Balaji C. Essentials of Radiation Heat Transfer. 1st ed. Cham: Springer International Publishing; 2021.
[8] Hagqvist P, Sikström F, Christiansson A. Emissivity estimation for high temperature radiation pyrometry on Ti–6Al–4V. Measurement 2013; 46: pp. 871–880.
[9] Wille G, Millot F, Rifflet JC. Thermophysical Properties of Containerless Liquid Iron up to 2500 K. Int. J. Thermophys. 2002; 23: pp. 1197–1206.
[10] Furumoto T, Ueda T, Alkahari MR, Hosokawa A. Investigation of laser consolidation process for metal powder by two-color pyrometer and high-speed video camera. CIRP Annals 2013; 62: pp. 223–226.
[11] Schöpp H, Sperl A, Kozakov R, Gött G, Uhrlandt D, Wilhelm G. Temperature and emissivity determination of liquid steel S235. J. Phys. D: Appl. Phys. 2012; 45: #235203.
[12] Taunay PCR, Choueiri EY. Multi-wavelength pyrometry based on robust statistics and cross-validation of emissivity model. Rev. Sci. Instrum. 2020; 91: #114902.
[13] Hua T, Jing C, Xin L, Fengying Z, Weidong H. Research on molten pool temperature in the process of laser rapid forming. J. Mater. Process. Technol. 2008; 198: pp. 454–462.
[14] Mates S, Basak D, Biancaniello F, Ridder S, Geist J. Calibration of a two-color imaging pyrometer and its use for particle measurements in controlled air plasma spray experiments. J. Therm. Spray Technol. 2002; 11: pp. 195–205.
[15] Araújo A. Multi-spectral pyrometry—a review. Meas. Sci. Technol. 2017; 28: #082002.
[16] Felice RA, Nash DA. Pyrometry of materials with changing, spectrally-dependent emissivity - Solid and liquid metals. Proc. AIP 2013; 1552: pp. 734–739.
[17] Song L, Mazumder J. Feedback Control of Melt Pool Temperature During Laser Cladding Process. IEEE Trans. Contr. Syst. Technol. 2011; 19: pp. 1349–1356.
[18] Bi G, Sun CN, Gasser A. Study on influential factors for process monitoring and control in laser aided additive manufacturing. J. Mater. Process. Technol. 2013; 213: pp. 463–468.
[19] Medrano A, Folkes J, Segal J, Pashby I. Fibre laser metal deposition with wire: parameters study and temperature monitoring system. Proc. SPIE 2009; 7131: pp. 1–7.
[20] Nair AM, Muvvala G, Sarkar S, Nath AK. Real-time detection of cooling rate using pyrometers in tandem in laser material processing and directed energy deposition. Mater. Lett. 2020; 277: #128330.
[21] Zapata A, Bernauer C, Stadter C, Kolb CG, Zaeh MF. Investigation on the Cause-Effect Relationships between the Process Parameters and the Resulting Geometric Properties for Wire-Based Coaxial Laser Metal Deposition. Metals 2022; 12: #455.